New physical implications from revisiting foreshock activity in southern California

Ester Manganiello[1], Marcus Herrmann[1], and Warner Marzocchi[1]

[1]Dipartimento di Scienze della Terra, dell'Ambiente e delle Risorse, Università degli Studi di Napoli 'Federico II', Naples, Italy

Corresponding author: E. Manganiello, ester.manganiello@unina.it

Key Points:

- We compare the foreshock activity in southern California with the prediction of the best-performing earthquake clustering model.
- Sequences with an anomalous excess of foreshocks are associated mostly with moderate mainshocks and preferentially with high heat flow.
- The prevalence of anomalous foreshock sequences in zones of high heat flow does not support the pre-slip nucleation model.

Abstract

Foreshock analysis promises new insights into the earthquake nucleation process and could potentially improve earthquake forecasting. Well-performing clustering models like the Epidemic-Type Aftershock Sequence (ETAS) model assume that foreshocks and general seismicity are generated by the same physical process, implying that foreshocks can be identified only in retrospect. However, several studies have recently found higher foreshock activity than predicted by ETAS. Here, we revisit the foreshock activity in southern California using different statistical methods and find anomalous foreshock sequences, i.e., those unexplained by ETAS, mostly for mainshock magnitudes below 5.5. The spatial distribution of these anomalies reveals a preferential occurrence in zones of high heat flow, which are known to host swarm-like seismicity. Outside these regions, the foreshocks generally behave as expected by ETAS. These findings show that anomalous foreshock sequences in southern California do not indicate a pre-slip nucleation process, but swarm-like behavior driven by heat flow.

Plain Language Summary

Many studies have observed that large earthquakes are preceded by smaller events, called foreshocks. If they have distinctive characteristics that make them recognizable in an ongoing sequence in real time, they can significantly improve the forecasting capability of large earthquakes. To investigate the nature of foreshocks, we compare real seismicity with the expectation of the most skilled earthquake clustering model, which assumes that foreshocks do not have any distinctive characteristics with respect to general seismicity. We find that discrepancies between reality and expectation mostly affect foreshock sequences that anticipate moderate mainshocks with magnitudes below 5.5. We show that those anomalous foreshock sequences tend to occur where the heat flow is high, which are already known for the occurrence of swarm-like sequences. Outside these regions, the observed foreshock activity is explained well by the clustering model. These findings indicate that anomalous foreshock sequences are not diagnostic of impending large earthquakes but are influenced by the heat flow.

1 Introduction

It is well known that many large earthquakes are preceded by smaller events (e.g., 1999 M7.6 Izmit, Turkey (Bouchon et al., 2011; Ellsworth & Bulut, 2018), 2009 M6.1 L'Aquila, Italy (Chiaraluce et al., 2011), 2011 M9.0 Tohoku, Japan (Kato et al., 2012), 2019 M7.1 Ridgecrest, USA (Meng & Fan, 2021)), which are (a posteriori) called foreshocks. The role of foreshocks in earthquake predictability can be epitomized by two still debated conceptual hypotheses about earthquake nucleation: the "pre-slip model" versus the "cascade model" (Ellsworth & Beroza, 1995; Gomberg, 2018). According to the former, foreshocks are diagnostic precursors, because they are triggered by an aseismic slip that precedes large earthquakes; in the latter model, foreshocks are like any other earthquake, which trigger one another, with one of them eventually becoming exceedingly larger (the mainshock).

Notwithstanding the still active debate on these hypotheses, seismologists are not yet able to recognize foreshocks in real-time, tacitly implying that foreshocks are not different from the rest of seismicity, indirectly supporting the cascade model. This view is further supported by the fact that the current best performing short-term earthquake forecasting model (Taroni et al., 2018)—the Epidemic-Type Aftershock Sequences (ETAS; Ogata, 1988) model—assumes that foreshocks, mainshocks, and aftershocks are undistinguishable and governed by the same

process. ETAS belongs to the class of branching point process models known in the statistical literature as Hawkes or self-exciting point processes: every earthquake can trigger other earthquakes according to established empirical relations, with their magnitudes being independent from past seismicity. In essence, ETAS implicitly acknowledges the cascade model and its good forecasting performance makes ETAS an appropriate null hypothesis.

Instead, if foreshocks are dominated by mechanisms other than earthquake triggering, as the pre-slip model expects, they could be distinguished from general seismicity and potentially increase the probability for a larger earthquake to follow. Several studies recently investigated foreshock sequences of southern California and found that they deviate from expectations of the classical ETAS model with spatially invariant parameters. For example, Seif et al. (2019), Petrillo and Lippiello (2021), and Moutote et al. (2021) find, albeit at varying degrees, a higher foreshock activity in real seismicity than in synthetic catalogs simulated with ETAS. Hence, ETAS appears to be unable to predict all the observed seismicity, which may suggest that foreshocks are distinct from general seismicity and governed by different mechanisms. These findings provide hope that foreshocks are distinguishable and could pave the way to significantly improved earthquake predictability.

Here we reexamine foreshock activity in southern California and investigate the existence and main characteristics of foreshock sequences that cannot be explained by ETAS, i.e., anomalous foreshock sequences. In other words, we look for evidence against the cascade model. To make the results comparable to previous analyses, we use an ETAS model with spatially invariant triggering parameters. We perform two different statistical tests and consider the potential influence of subjective choices, such as the method to identify mainshocks and their foreshocks. To fathom the main characteristics of possible anomalous foreshock sequences, we investigate different magnitude classes and analyze the spatial correlation with heat flow as a physical parameter. With our findings, we aim to contribute to improving earthquake forecasting and the understanding of earthquake nucleation processes.

2 Data and Methods

We use the relocated earthquake catalog for southern California catalog (Hauksson et al., 2012, see Data Availability Statement), selecting all earthquakes with $M \geq 2.5$ from 1-1-1981 to 31-12-2019 except nuclear events (i.e., at the Nevada Test site) from the catalog, totaling 47'574 events.

Because there is no absolute and precise procedure to identify mainshocks, foreshocks, and aftershocks, the way of analyzing a catalog and distinguishing these events is unavoidably subjective (Molchan & Dmitrieva, 1992; Zaliapin et al., 2008). To mitigate this subjective choice, we analyze the catalog using two quite different techniques: the Nearest-Neighbor (NN) clustering analysis proposed by Baiesi and Paczuski (2004) and elaborated by Zaliapin et al. (2008), and the spatiotemporal windows (STW) method (Agnew and Jones, 1991; Marzocchi and Zhuang, 2011; Seif et al., 2019).

The NN method operates in a space-time-magnitude domain based on the NN distance η_j, i.e., the space-time-magnitude distance between event j and all earlier events i that is minimal. The event i with the shortest distance to event j is called NN, or parent, event. By assigning a parent event to each event j, all events become associated with another. To identify individual families (i.e., sequences) or single events, we use the same threshold $\eta_0 = 10^{-5}$ as Zaliapin et al.

(2008), which effectively removes event associations with too large η_j. For each sequence, we refer to the event with the largest magnitude as the mainshock and all associated events that occur before it as its foreshocks. We only consider sequences with foreshocks and ignore those that have no foreshocks.

For the STW method, we initially consider all events with magnitude $M \geq 4$ as possible mainshocks. Then, we exclude events that are (i) preceded by a larger event within a spatiotemporal window of 10 km and 3 days; (ii) preceded by an event with $M > 5$ within 100 km and 180 days; and (iii) not preceded by at least one event within 10 km and 3 days. For the remaining mainshocks, all preceding events within a window of 10 km and 3 days are considered foreshocks.

To simulate synthetic catalogs, we use the ETAS model of K. Felzer (Felzer et al., 2002, see Data Availability Statement and supporting information Text S1 and Table S1) with spatially invariant triggering parameters given by Hardebeck et al. (2008, see Table S2). Using an available ETAS model reduces potential influences from subjective parameter choices. We verify its overall reliability by comparing the number of events in the real catalog with the distribution of simulated events in the synthetic catalogs (see Text S2 and Figures S1 and S2), finding that the ETAS model is consistent with the observation.

Once the mainshocks and their foreshocks have been identified in both the real and 1000 synthetic catalogs, we compare their foreshock statistics using two approaches named TEST1 and TEST2. The two tests are described in detail below; both use the cascade model, which is implied by ETAS, as null hypothesis but emphasize different aspects of the problem. TEST1 involves the average number of observed foreshocks per sequence, whereas TEST2, which has been inspired by the work of Seif et al. (2019), involves the frequency of observing a certain number of foreshocks per sequence. We apply both tests to various mainshock magnitude classes $C_\mathrm{M} = \{4.0 \leq m_\mathrm{M} < 4.5, 4.5 \leq m_\mathrm{M} < 5.0, 5.0 \leq m_\mathrm{M} < 5.5, 5.5 \leq m_\mathrm{M} < 6.0, m_\mathrm{M} \geq 6.0\}$ and foreshock magnitude thresholds $T_\mathrm{F} = \{m_\mathrm{F} \geq 2.5, m_\mathrm{F} \geq 3.0, m_\mathrm{F} \geq 3.5, m_\mathrm{F} \geq 4.0\}$; these choices are based on Seif et al. (2019), but we add the class $4.0 \leq m_\mathrm{M} < 4.5$ to C_M. Although we report statistical test results, we do not formally account for applying the tests multiple times; the results are therefore meant to indicate possible patterns of (apparently) anomalous foreshock activity.

In TEST1, the null hypothesis under test $H_0^{(1)}$ is that the average number of foreshocks in the real catalog is not larger than the corresponding quantity in the synthetic catalogs. For each mainshock magnitude class $\mathrm{c} \in C_\mathrm{M}$ and each foreshock magnitude threshold $\mathrm{t} \in T_\mathrm{F}$, we count the number of mainshocks (with foreshocks), $N_\mathrm{M}^\mathrm{real}$, and the number of foreshocks $N_\mathrm{F}^\mathrm{real}$ in the real catalog; $N_\mathrm{F}^\mathrm{real}$ is normalized by $N_\mathrm{M}^\mathrm{real}$ to obtain $\widehat{N}_\mathrm{F}^\mathrm{real}$. We calculate the same quantity for each synthetic catalog and build its empirical cumulative distribution function (eCDF); if $\widehat{N}_\mathrm{F}^\mathrm{real}$ is above the 99$^\mathrm{th}$ percentile of the eCDF, we reject $H_0^{(1)}$ at a significance level of 0.01.

In TEST2, the null hypothesis under test $H_0^{(2)}$ is that for each number of foreshocks, $N_\mathrm{F} > 0$, the frequency of observed cases is not larger than the frequency in synthetic catalogs. For each $c \in C_\mathrm{M}$ and each $t \in T_\mathrm{F}$, we count the number of mainshocks that have a certain N_F and normalize it by $N_\mathrm{M}^\mathrm{real}$. In this way, we obtain the probability mass function (PMF) for the real catalog as a function of N_F. Then, we apply the same procedure to each synthetic catalog and obtain 1000

synthetic PMFs, for which we calculate the 99th percentile at each N_F. Finally, at each N_F, we reject $H_0^{(2)}$ at a significance level of 0.01 if the corresponding PMF value of the real catalog is larger than the 99th percentile (i.e., when the real catalog contains more foreshock sequences with this specific N_F than expected by ETAS). In essence, TEST2 seeks anomalies at every N_F, whereas TEST1 could be seen as a cumulative version of TEST2.

Based on the results of the tests, we can label each foreshock sequence as 'anomalous' or 'normal' using an intuitive approach: for TEST1, if the null hypothesis is rejected for a certain class, all foreshock sequences with a N_F larger than the 99th percentile of the eCDF in that class are labeled as 'anomalous' (and 'normal' otherwise); for TEST2, if the null hypothesis is rejected for a specific N_F, all sequences with this N_F are labeled as 'anomalous' (and 'normal' otherwise). Effectively, a foreshock sequence in $c \in C_M$ is labeled 'anomalous' if it is 'anomalous' in at least one class $t \in T_F$. For TEST1, we argue that the approach is conservative, because comparing a single sequence against the average behavior of foreshock sequences may lead to wrongly label more actual normal foreshock sequences as 'anomalous' (i.e., false positives) than wrongly labeling anomalous foreshock sequences as 'normal' (i.e., false negatives). To investigate this aspect, we perform an alternative analysis by building two eCDFs of N_F (i.e., without normalizing by N_M): one for the real catalog ($eCDF^{real}$) and one for all synthetic catalogs combined ($eCDF^{ETAS}$). If the 99th percentile of $eCDF^{real}$ is larger than the corresponding percentile of $eCDF^{ETAS}$ in a certain class, we label each foreshock sequence as 'anomalous' whose N_F is above the 99th percentile of $eCDF^{ETAS}$.

To investigate the physical interpretation of possible anomalous foreshock sequences in the real catalog, we analyze their spatial distribution. Specifically, taking inspiration from Zaliapin and Ben-Zion (2013), we create a map by interpolating heat flow measurements (see Data Availability Statement) with a radial smoothing approach ($r = 20$ km) to acknowledge areas without data. For each foreshock sequence, we extract the interpolated heat flow value closest to the mainshock location if it is within *r,* otherwise we discard the sequence. Then we test if the distribution of extracted heat flow values is significantly different for normal and anomalous foreshock sequences. If pre-slip is responsible for anomalous foreshock sequences, we should not find any difference, i.e., a spatial pattern. We employ two statistical tests: the two-sample Kolmogorov-Smirnov test (null hypothesis: the two distributions have the same parent distribution), and the paired Wilcoxon test (null hypothesis: the two distributions have the same median). In essence, the Kolmogorov-Smirnov test is sensitive to any kind of difference between both distributions, whereas the Wilcoxon test is sensitive to one distribution having higher values than the other.

3 Results

3.1 Testing for anomalous foreshock activity

Figure 1 shows the results of TEST1 using NN to identify mainshocks and their foreshocks; the results using STW are reported in supporting information Figure S3. Each subplot shows a comparison of the eCDF based on synthetic catalogs with the observed value from the real catalog for each class in C_M and T_F. As shown in Figure 1 and Figure S3, TEST1 rejects $H_0^{(1)}$, i.e., identifies anomalous foreshock sequences, exclusively for mainshock magnitudes $m_M <$ 5.5. Of a total of 152 foreshock sequences, we find 61 (40%) to be anomalous; with the STW method we find 143 foreshock sequences of which 34 (23%) are anomalous (all with $m_M <$

187 5.5.). Using instead the alternative analysis without normalizing by N_M (Figure S4), we find 19
188 (12.5%) to be anomalous, which suggests that TEST1 overestimated the number of anomalies
189 due to using averages, as anticipated in Data and Methods.

190 Figure 2 shows the results of TEST2 for each class in C_M and T_F using the NN method; the
191 results using the STW method are reported in supporting information Figure S5. Most PMF
192 values of the real catalog are not anomalous because they are below the 99th percentile of
193 synthetic PMF values. We find 21 of 152 (14%) foreshock sequences to be anomalous, most of
194 which are again associated with $m_M < 5.5$ (only three have larger m_M). Using the STW method
195 we find 10 of 143 (7%) foreshock sequences to be anomalous.

196 For comparison, Figure 2 also reports the results obtained by applying the approach of Seif et al.
197 (2019), which tests a similar yet different null hypothesis than TEST2. Specifically, they treat all
198 synthetic catalogs as one single compound catalog. In this way, the PMF is normalized with a
199 much larger number of mainshocks than a single catalog (e.g., like the real catalog); for an
200 increasing number of synthetic catalogs, the PMF decreases progressively observation (i.e.,
201 lowering the detectable minimum frequency) and moves further away from the real. In other
202 words, our TEST2 honors the fact that a finite earthquake catalog must have a lower detectable
203 frequency of foreshocks in the PMF; this lower frequency depends on the number of mainshocks
204 that have foreshocks, which in turn depends on the length of the earthquake catalog (the lowest
205 frequency is 1 out of the number of mainshocks that have foreshocks). In addition, the approach
206 of Seif et al. (2019) normalizes the PMF by the total number of mainshocks that have foreshocks
207 (N_M, as we do in TEST2) *and* no foreshocks, which further reduces the PMF by another 0.5–1
208 order of magnitude depending on $c \in C_M$.

209 We repeated TEST1 and TEST2 at a 0.05 significance level (i.e., 95th percentile), which was
210 originally used by Seif et al. (2019), see supporting information (Text S3 and Figures S6 and
211 S7).

212 3.2 Correlating foreshock sequences with the heat flow

213 To investigate the physical cause of anomalous foreshock sequences we inspect the correlation
214 of their locations with the local heat flow. We choose this property because previous papers
215 suggested that the heat flow relates to statistical properties of seismic sequences (e.g., Enescu et
216 al., 2009, Chen & Shearer, 2016; Ross et al., 2021; Zaliapin & Ben-Zion, 2013).

217 Figures 3a and 4a overlay the locations of normal and anomalous foreshock sequences identified
218 by TEST1 and TEST2, respectively, on a heat flow map. Figures 3b and 4b show the
219 corresponding eCDFs of the interpolated heat flow observed at the locations of normal and
220 anomalous foreshock sequences. In both cases, anomalous foreshock sequences tend to occur
221 more frequently at locations of higher heat flow than normal sequences. This trend is confirmed
222 by the *p*-values of the two-sample Kolmogorov-Smirnov and paired Wilcoxon tests (see
223 annotations in Figures 3b and 4b), which are below 0.05, indicating that the two samples come
224 from different parent distributions with different means. Figures 3 and 4 are based on the NN
225 method to identify mainshocks and their foreshocks; the results based on the STW method
226 confirm our findings (see supporting information Figures S8 and S9), as do the results based on a
227 0.05 significance level (Figures S10 and S11). Moreover, TEST1-based results are stable even if
228 we use the alternative procedure to identify anomalous foreshock sequences using eCDFs
229 without normalizing by N_M (see Figure S12).

We verify the stability of our results using foreshock anomalies identified by Petrillo and Lippiello (2021). The authors provided us locations of their identified normal and anomalous foreshock sequences (G. Petrillo, pers. comm., 2022), letting us apply our analysis on a dataset that is completely independent from our assumptions and modeling choices. The results shown in Figure S13 confirm our findings of a preferential occurrence of foreshock anomalies in zones of high heat flow.

Finally, we add a word of caution on the interpretation of the results, that is, the spatial coverage of heat flow data compared to the earthquake activity is rather incomplete in northern Mexico. For instance, several anomalous foreshock sequences occur in this area but cannot be included in the heat flow analysis due to the lack of heat flow measurements. In addition, the available heat flow measurements in northern Mexico are not consistent with the Geothermal map of North America (Blackwell & Richards, 2004), which indicates a generally high heat flow (> 100 $\mu W/m^2$) in this area along the San Andreas Fault.

4 Discussion & Conclusion

We have found that foreshocks have the same characteristics of general seismicity as expected by ETAS, except for some cases. Our finding is in general agreement with previous studies of foreshock activity, all of which found (with some important differences not discussed here) higher foreshock activity than expected (Chen & Shearer, 2016; Moutote et al., 2021; Petrillo & Lippiello, 2021; Seif et al., 2019). However, our results additionally show that foreshock anomalies are mostly associated with mainshock magnitudes below 5.5—independently from the two tests and the two procedures to identify mainshocks and their foreshocks. Moreover, these anomalies are located preferentially (and statistically significant) in zones of high heat flow. The combination of these two findings suggests that sequences with anomalous foreshock activity behave more like seismic swarms. In fact, independent studies (e.g., Enescu et al., 2009, Chen & Shearer, 2016; Ross et al., 2021; Zaliapin & Ben-Zion, 2013) have shown that swarm-like activity is common in those areas where we have found anomalous foreshock sequences.

Our results do not allow us to further elucidate why foreshock anomalies correlate with high heat flow. The anomalies may be driven by specific physical mechanisms (e.g., actual seismic swarms mostly driven by fluids) or still relate to a cascade model that is not spatially uniform. The latter may be better described by an ETAS model with spatially varying triggering parameters. In fact, Enescu et al. (2009) and Nandan et al. (2017) show that some parameters of a spatially varying ETAS model (which mostly depend on the more abundant aftershocks) correlate with the heat flow in southern California. Such a more elaborated clustering model implies more active foreshock sequences where the heat flow is high, which agrees with our empirical findings based on the analysis of (less abundant) foreshocks.

Conversely, foreshock sequences located in zones of lower heat flow predominantly behave as expected, i.e., in agreement with the null hypothesis given by the ETAS model. Since it is reasonable to assume that a pre-slip model should not be severely affected by heat flow, our results do not indicate the pre-slip model as a major candidate to explain the anomalous foreshock behavior in southern California. It goes without saying that our results do not prove the cascade model as the truth, but that they do not bring any evidence against it and in favor of the pre-slip model.

Our results also highlight the importance of analyzing seismic sequences in zones of high heat flow in more detail, especially to understand the physical reasons of anomalous foreshock sequences: Are they related to seismic swarms with an implicit limitation to the mainshock magnitude? Or are they related to different clustering processes than those driving tectonic sequences? The difference is crucial, in particular regarding the forecasting of large earthquakes.

Our findings raise an urgent need to find (quasi-)real-time methods to discriminate swarm-like from ETAS-like sequences. Such a discrimination method could lead to significant improvements in earthquake forecasting, because being able to identify a swarm-like sequence as such could markedly reduce the forecast probability for a large earthquake. We note that an interesting attempt in this direction has been made by Zaliapin and Ben-Zion (2013), who found that swarm-like sequences have a different topologic tree structure (i.e., an internal clustering hierarchy, which connects background and triggered earthquakes). Unfortunately, this method can currently only be used retrospectively, limiting its applicability in earthquake forecasting. We envision other possible parameterizations of the topologic tree structure that may facilitate its use from a forecasting perspective.

Acknowledgments

We thank Luc Moutote and an anonymous reviewer for their very useful suggestions, which significantly helped improving the article. We also thank G. Petrillo for providing us with independent data. This project has received funding from the European Union's Horizon 2020 research and innovation program under Grant Agreement Number 821115, *Real-Time Earthquake Risk Reduction for a Resilient Europe* (RISE).

Open Research

The southern California catalog of Hauksson et al. (2012) was obtained from https://scedc.caltech.edu/data/alt-2011-dd-hauksson-yang-shearer.html, version "1981–2019" (last accessed April 2021). Heat flow data were obtained from the following sources: National Geothermal Data System (http://geothermal.smu.edu/static/DownloadFilesButtonPage.htm, last accessed May 2021) using the data sets '*Aggregated Well Data*', '*Heat Flow Observation in Content Model Format*', '*SMU Heat Flow Database of Equilibrium Log Data and Geothermal Wells*', and '*SMU Heat Flow Database from BHT Data*'; and RE Data Explorer (https://www.re-explorer.org/re-data-explorer/download/rede-data, last accessed May 2021) for northern Mexico. The ETAS simulator of K. Felzer was obtained from https://web.archive.org/web/20200712004939/https://pasadena.wr.usgs.gov/office/kfelzer/AftSimulator.html, last accessed February 2022). The alternative dataset of normal and anomalous foreshock locations was provided by G. Petrillo (pers. comm., 2022). The methods to perform our foreshocks analyses are available as MATLAB code at DOI: 10.5281/zenodo.6376221 and https://gitlab.com/ester.manganiello/foreshock-analyses.

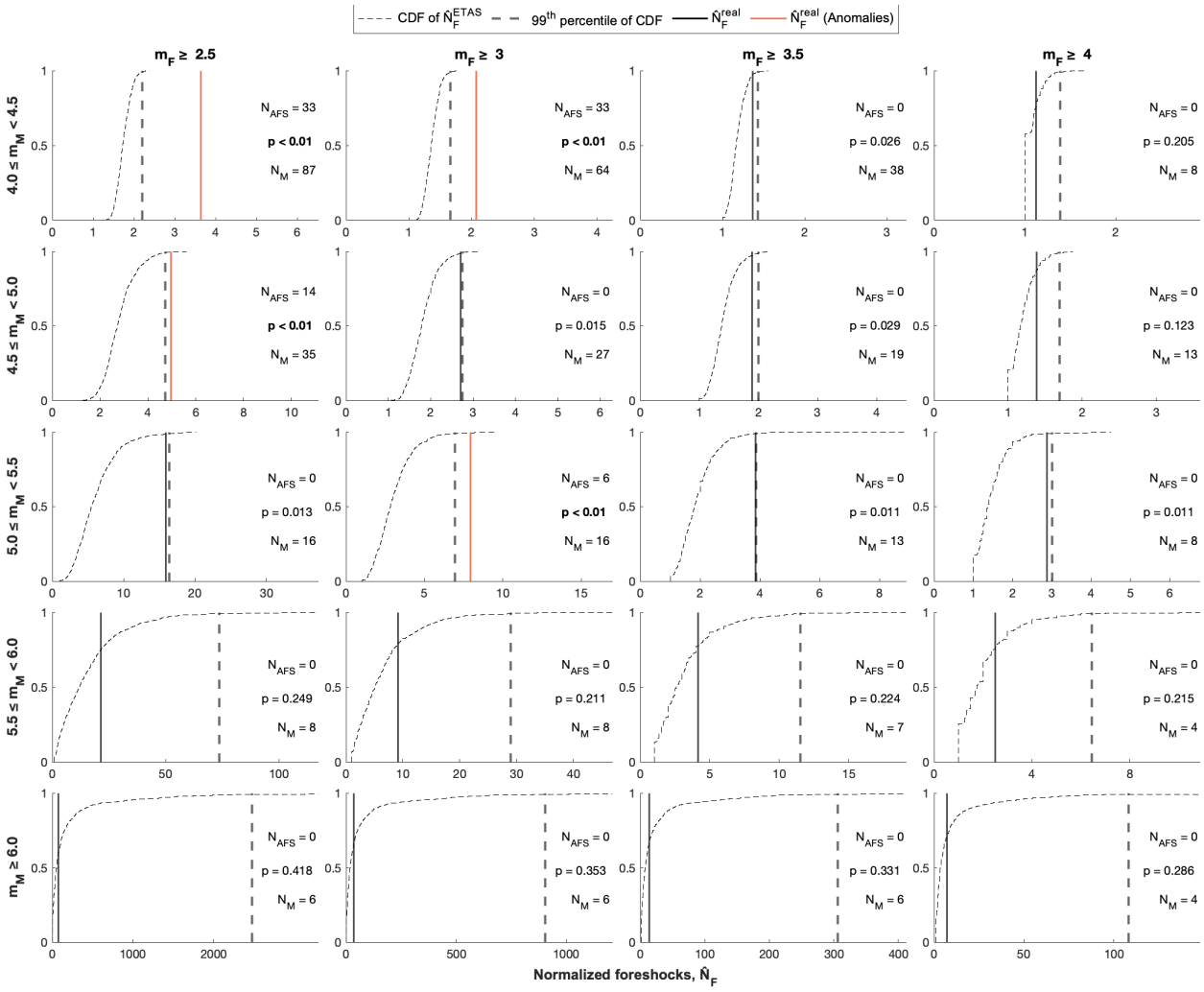

Figure 1. Results of TEST1 for various classes of the mainshock magnitude m_{M} (rows) and thresholds for the foreshock magnitude m_{F} (columns). Each subplot displays the number of normalized foreshocks $\widehat{N}_{\mathrm{F}}$ for the real catalog (vertical lines; red if anomalous, black otherwise) and the empirical Cumulative Distribution Functions (eCDFs, dashed curves) with its 99$^{\mathrm{th}}$ percentile (dashed vertical lines) for 1000 synthetic catalogs. Each subplot also reports the number of anomalous foreshock sequences, N_{AFS}, the p-value for TEST1, and the number of mainshocks, N_{M}. The results are based on the NN method; supporting information Figure S3 shows results based on the STW method. Note that each subplot uses a different N_{F}-axis range to account for the varying data range.

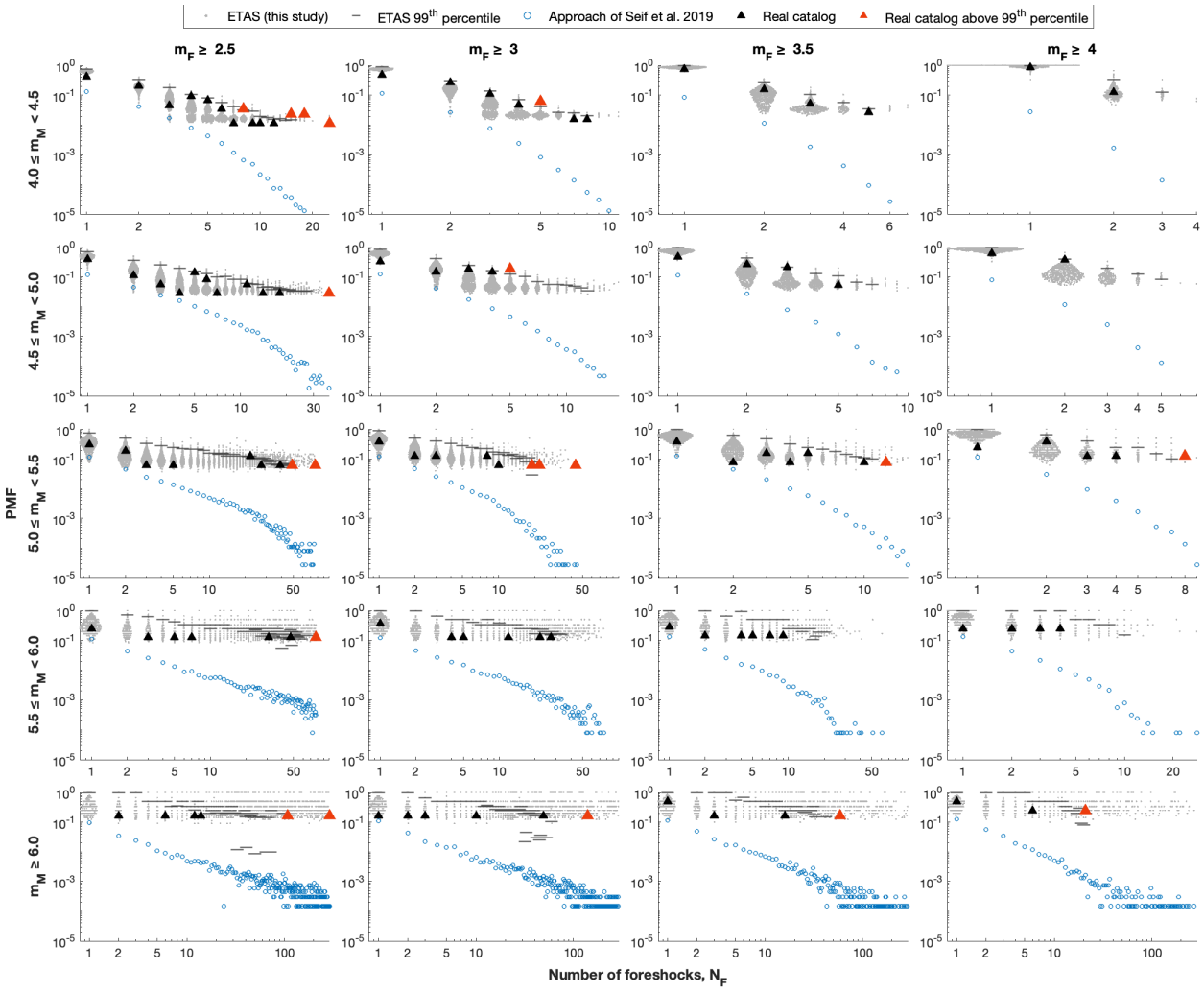

Figure 2. Results of TEST2 showing probability mass functions (PMFs) of the number of foreshocks N_F for various classes of m_M (rows) and m_F (columns). The PMFs are shown for (i) the real catalog (triangles), (ii) all synthetic catalogs (small gray dots as swarm distributions) with their 99th percentile (gray horizontal bars), and (iii) when considering all synthetic catalogs as a single compound catalog (blue open circles, using the approach of Seif et al., 2019). Triangles become red when they are located above the 99th percentile of (ii). The results are based on the NN method to identify mainshocks and their foreshocks; supporting information Figure S5 shows results based on the STW method. Note that each subplot uses a different N_F-axis range.

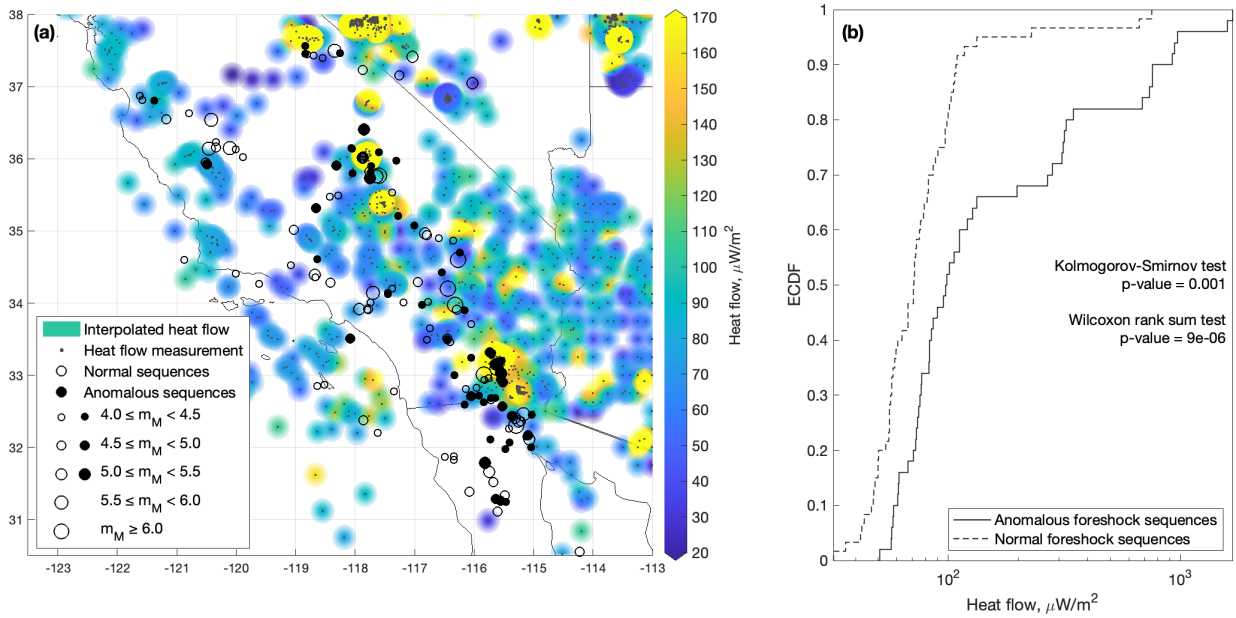

Figure 3. Correlating foreshock sequences with the heat flow. (a) Locations of normal (empty circles) and anomalous foreshock sequences (filled circles) identified with TEST1 overlayed on a heat flow map. The circles sizes scales with m_{M} (see legend). The interpolated heat flow map is based on sampled heat flow measurements (small gray dots, see Data and Methods section); (b) eCDFs of heat flow values at locations of normal (dashed curve) and anomalous foreshock sequences (solid curve); both eCDFs are compared using two statistical tests (see annotation with corresponding *p*-values). The results are based on the NN method; supporting information Figure S8 shows results based on the STW method.

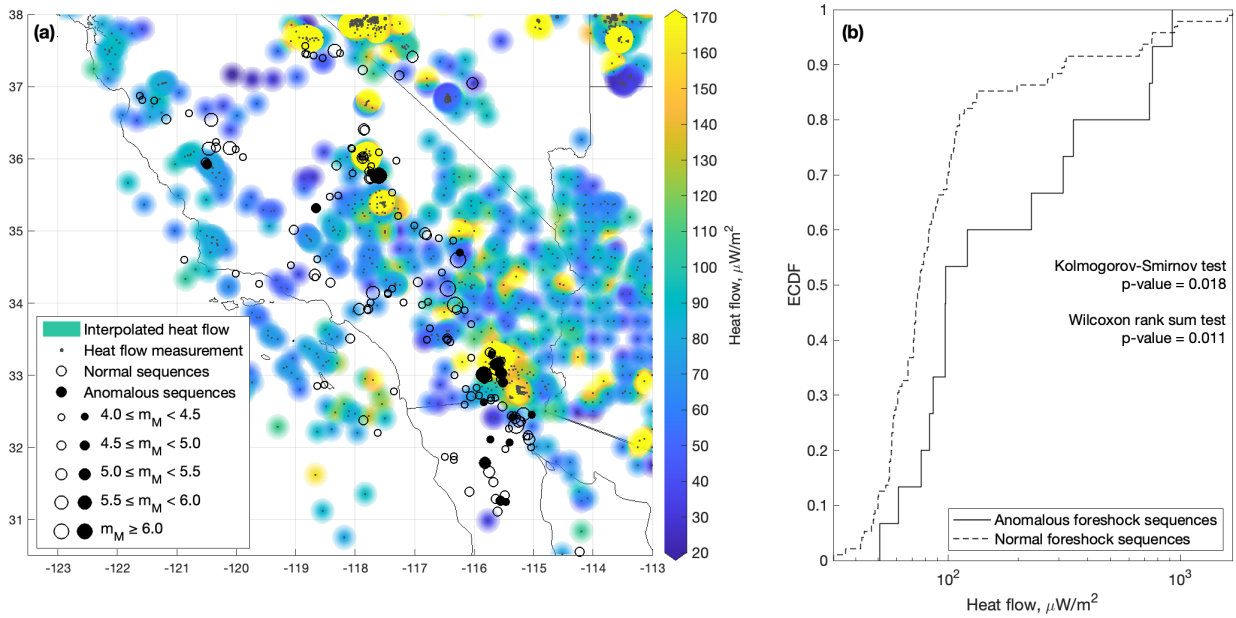

Figure 4. Like Figure 3 but with foreshock sequences labeled as 'anomalous' or 'normal' using TEST2. Supporting information Figure S9 shows results based on the STW method.

References

Agnew, D. C., & Jones, L. M. (1991). Prediction probabilities from foreshocks. *Journal of Geophysical Research, 96*(B7), 11959. https://doi.org/10.1029/91JB00191

Baiesi, M., & Paczuski M. (2004). Scale-free networks of earthquakes and aftershocks. *Physical Review E*, *69*, 066106. https://doi.org/10.1103/PhysRevE.69.066106.

Blackwell, D. D., & Richards, M. (2004). Geothermal Map of North America, AAPG Map, scale 1:6,500,000, Product Code 423. url: https://www.smu.edu/-/media/Site/Dedman/Academics/Programs/Geothermal-Lab/Graphics/Geothermal_MapNA_7x10in.gif

Bouchon, M., Karabulut, H., Aktar, M., Özalaybey, S., Schmittbuhl, J., & Bouin, M. P. (2011). Extended Nucleation of the 1999 Mw 7.6 Izmit Earthquake. *Science*, *331*(6019), 877–880. https://doi.org/10.1126/science.1197341

Chen, X. & Shearer, P. M. (2016). Analysis of Foreshock Sequences in California and Implications for Earthquake Triggering. *Pure Applied Geophysical*, *173*(1), 133–152. https://doi.org/10.1007/s00024-015-1103-0

Chiaraluce, L., Chiarabba, C., De Gori, P., Di Stefano, R., Improta, L., Piccinini, D., Schlagenhauf, A., Traversa, P., Valoroso, L., & Voisin, C. (2011). The 2009 L'Aquila (central Italy) seismic sequence. *Bollettino di Geofisica Teorica ed Applicata*, *52*(3), 367-387. https://doi.org/10.4430/bgta0019

Ellsworth, W. L., & Beroza, G. C. (1995). Seismic Evidence for an Earthquake Nucleation Phase. *Science*, *268*, 851-855. https://doi.org/10.1126/science.268.5212.851

Ellsworth, W. L., & Bulut, F. (2018). Nucleation of the 1999 Izmit earthquake by a triggered cascade of foreshocks. *Nature Geoscience*, *11*(7), 531–535. https://doi.org/10.1038/s41561-018-0145-1

Enescu, B., Hainzl, S., and Ben-Zion, Y. (2009). Correlations of Seismicity Patterns in Southern California with Surface Heat Flow Data. *Bulletin of the Seismological Society of America*, *99* (6), 3114-3123. https://doi.org/10.1785/0120080038

Felzer, K. R., Becker, T. W., Abercrombie, R. E., Ekström, G., & Rice, J. R. (2002). Triggering of the 1999 M_w 7.1 Hector Mine earthquake by aftershocks of the 1992 M_w 7.3 Landers earthquake. *Journal of Geophysical Research*, *107*(B9), 2190. https://doi.org/10.1029/2001JB000911

Gomberg, J. (2018). Unsettled earthquake nucleation. *Nature Geoscience*, 11(7), 463–464. https://doi.org/10.1038/s41561-018-0149-x

Hardebeck, J. L., Felzer, K. R., & Michael, A. J. (2008). Improved tests reveal that the accelerating moment release hypothesis is statistically insignificant. *Journal of Geophysical Research*, *113*, 3B08310. https://doi.org/10.1029/2007JB005410

Hauksson, E., Yang, W., & Shearer, P. M. (2012). Waveform relocated earthquake catalog for Southern California (1981 to June 2019). *Bulletin of the Seismological Society of America*, *102*(5), 2239–2244. https://doi.org/10.1785/0120120010

Kato, A., Obara, K., Igarashi, T., Tsuruoka, H., Nakagawa, S., & Hirata, N. (2012). Propagation of Slow Slip Leading Up to the 2011 Mw 9.0 Tohoku-Oki Earthquake. *Science*, *335*(6069), 705-708. https://doi.org/10.1126/science.1215141

Marzocchi, W., & Zhuang, J. (2011). Statistics between mainshocks and foreshocks in Italy and Southern California. *Geophysical Research Letters*, *38*(9), 2011GL047165. https://doi.org/10.1029/2011GL047165

386 Meng, H., & Fan, W. (2021). Immediate foreshocks indicating cascading rupture developments
387 for 527 M 0.9 to 5.4 Ridgecrest earthquakes. *Geophysical Research Letters*, *48*,
388 e2021GL095704. https://doi.org/10.1029/2021GL095704
389 Molchan, G. M., & Dmitrieva, O. E. (1992). Aftershock identification: methods and new
390 approaches. *Geophysical Journal International*, *109*(3), 501–516.
391 https://doi.org/10.1111/j.1365-246X.1992.tb00113.x
392 Moutote, L., Marsan, D., Lengliné, O., & Duputel, Z. (2021). Rare occurrences of non-cascading
393 foreshock activity in Southern California. *Geophysical Research Letters*, *48*,
394 e2020GL091757. https://doi.org/10.1029/2020GL091757
395 Nandan, S., Ouillon, G., Wiemer, S., and Sornette, D. (2017). Objective estimation of spatially
396 variable parameters of epidemic type aftershock sequence model: Application to
397 California, *Geophysical Research Letters Solid Earth*, *122*, 5118–5143.
398 https://doi.org/10.1002/2016JB013266
399 Ogata, Y. (1988). Statistical models for earthquake occurrences and residual analysis for point
400 processes. Journal of the American Statistical Association, 83 (401), 9-27.
401 https://doi.org/10.1080/01621459.1988.10478560
402 Petrillo, G., & Lippiello, E. (2021). Testing of the foreshock hypothesis within an epidemic like
403 description of seismicity. *Geophysical Journal International*, *225*, 1236–1257.
404 https://doi.org/10.1093/gji/ggaa611
405 Ross, Z. E, Cochran, E. S., Trugman, D. T., & Smith, J. D. (2021). 3D fault architecture controls
406 the dynamism of earthquake swarms. *Science*, *368*(6497), 1357-1361.
407 https://doi.org/10.1126/science.abb0779
408 Seif, S., Zechar, J. D., Mignan, A., Nandan, S., & Wiemer, S. (2019). Foreshocks and Their
409 Potential Deviation from General Seismicity. *Bulletin of the Seismological Society of*
410 *America*, *109* (1), 1–18. https://doi.org/10.1785/0120170188
411 Taroni, M., Marzocchi, W., Schorlemmer, D., Werner, M. J., Wiemer, S., Zechar, J. D.,
412 Heiniger, L., & Euchner, F. (2018). Prospective CSEP Evaluation of 1-Day, 3-Month,
413 and 5-Yr Earthquake Forecasts for Italy. *Seismological Research Letters*, *89*, 1251-1261.
414 https://doi.org/10.1785/0220180031
415 Zaliapin, I., & Ben-Zion, I. (2013). Earthquake clusters in southern California I: Identification
416 and stability. *Journal of Geophysical Research: Solid Earth*, *118*, 2847-2864.
417 https://doi.org/10.1002/jgrb.50179
418 Zaliapin, I., & Ben-Zion, I. (2013). Earthquake clusters in southern California II: Classification
419 and relation to physical properties of the crust. *Journal of Geophysical Research: Solid*
420 *Earth*, *118*, 2865-2877. http://doi.org/10.1002/jgrb.50178
421 Zaliapin, I., Gabrielov, A., Keilis-Borok, V., & Wong, H. (2008). Clustering Analysis of
422 Seismicity and Aftershock Identification. *Physical Review Letters*, *101*, 018501.
423 https://doi.org/10.1103/PhysRevLett.101.018501